Check for updates

White-light-driven plasmonic nanoparticle printing for opto-thermal manipulation and SERS application

Shreyas Mysuru Shivalingegowda (ID) and Sajan D. George (ID) *

The optical printing of nanoparticles from a colloidal solution is a simple and flexible approach and is currently being explored for printing plasmonic particles at desired locations. However, the practical application of such printed patterns is limited as it relies on focused laser beams for the bubble-assisted or direct printing of the nanoparticles. Here, we demonstrate the white-light-assisted printing of plasmonic nanoparticles and the utilization of the same for optothermally trapping the objects at desired locations *via* selective optical radiation exposure to a multi-patterned substrate. By combining the selective exposure and the optothermal force, the tweezing of the trapped object along the pre-defined paths is also illustrated. The surface-enhanced Raman spectroscopy studies carried out on the printed plasmonic patterns reveal that the printing time scale determines the Raman signal enhancement, and the optimized printed patterns provide a limit of detection of 62 pM for the probe molecule, crystal violet.

Introduction

The directed assembly of nanoparticles under external stimuli is an emerging area of research due to its applications in creating hierarchical architectures. Different kinds of external stimuli such as optical,[1,2] electrical,[3,4] magnetic,[5,6] and acoustic[7,8] stimuli have been employed to create such architectures. Among these, optical techniques wherein optical forces are used to capture nanoparticles and immobilize them onto the substrate are becoming increasingly popular due to their non-contact nature. Though optical forces can be applied to all kinds of nanoparticles, plasmonic nanoparticles are preferentially printed using optical techniques due to their plasmonic resonance matching with the excitation wavelength.[9–11] Researchers have fabricated well-controlled nanostructures of single spherical AuNPs,[12–14] aligned Au nanorods,[15–17] connected Au–Ag heterodimers,[18–20] and gold bipyramids.[2,21,22] In addition, by spatially modulating the light, simultaneous optical printing of multiple NPs is also illustrated.[23] We recently demonstrated the simultaneous and permanent optical printing of plasmonic Ag nanoparticles on both the floor and ceiling of a transparent chamber containing plasmonic colloidal solution using optically induced thermal and

scattering forces and investigated the influence of sample chamber thickness and laser power on both the printing mechanism and the resulting nanoparticle patterns.[24] In addition, we illustrated the printing of the plasmonic nanoparticles onto the tip of an optical fiber and its utilization for optothermally arresting biological cells.[25]

The optical printing mechanism relies on two phenomena: the interaction of optical radiation with nanoparticles and the interaction of the nanoparticles with the substrate. In the case of plasmonic nanoparticles, the nanoparticles along the propagation direction absorb the light and create a temperature gradient that takes the particles close to the substrate due to Marangoni flow, wherein the particles interact *via* van der Waals force to get anchored to the substrate.[26] Furthermore, researchers also utilized optomechanical coupling under a light-controlled electric field for the manipulation and printing of colloidal particles. In addition, the light-assisted tailoring of the photoconductivity of photoresponsive substrates,[27] entropically favorable photon–phonon conversion in optothermally thermally responsive materials,[28] thermophoresis or thermo-capillary Marangoni flow,[29] and light-controlled photochemical reaction[30] are used for the colloidal manipulation and optical printing of the nanoparticles. In comparison with the conventional top-down nanofabrication technique, this approach allows the assortment of nanoparticles and is devoid of the requirement of an expensive clean room facility. Aside from the usage of optical forces, the formation of vapor bubbles *via* heating of the solid–liquid interfaces is also used for the printing of plasmonic nanoparticles[31] and MXenes.[32]

Centre for Applied Nanosciences (CANs), Manipal Institute of Applied Physics, Manipal Academy of Higher Education, Manipal, 576104, India.
E-mail: sajan.george@manipal.edu

In this microbubble-assisted printing technique, the colloidal particles are attracted to the bubble *via* Marangoni convection and trapped at the bubble–liquid interface before immobilization to the substrate *via* van der Waals and electrostatic interactions. However, the control of printing nanoparticles from the colloidal solutions largely depends on the solvent composition and colloidal concentration. Nevertheless, these printed patterns are now finding increasing application in diverse areas, including optothermal trapping and surface-enhanced Raman spectroscopy.[33–35]

The major challenge in all these optical techniques is that all these processes are a point-by-point printing approach and are mostly carried out using a focused laser as the optical source. The utilization of lasers limits the area that can be covered and thus makes the printing process slow and expensive. To mitigate this, recently, we illustrated, for the first time, the white light from a commonly used projector light-assisted printing mechanism.[36] In this work, we investigated the temporal evolution of the optically printed pattern diameter and its transmittance. An application of the optically printed plasmonic pattern to trap objects such as yeast cells and the temporal stability of the trap are illustrated. Additionally, by selectively exposing the desired patterns onto a multi-pattern substrate, the possibility of the desired location trapping and the movement of the objects across the surface is investigated. In addition, the potential of printed regions in surface-enhanced Raman scattering is investigated, and it is observed that the printing time scale plays a critical role in the Raman signal enhancement of the probe molecule, crystal violet, investigated here.

Results and discussion

The temporal evolution of the plasmonically printed region from the Ag colloidal solution under optical illumination from a commercially available projector lamp that is coupled through amicroscope is imaged as a function of time, and the printed plasmonic patterns are shown in Fig. 1a(i–xii). The study reveals that at a given light irradiation power (~40 µW, measured using the integrated sphere at the glass–liquid interface) and a projected beam spot size of 6 µm, the printed region expands laterally and reaches a plateau region. As illustrated in Fig. 1b, the lateral dimension of the printed pattern diameter increases nearly exponentially in the lower time scales and reaches a saturation value of nearly 19 µm at 400 s, and further optical irradiation does not change the printed region dimensions. The transmitted power through the printed region is measured using an integrated sphere, and it is observed that the transmittance also exhibits a similar trend with a substantial reduction of transmitted intensity (nearly 71%) beyond 400 s (Fig. 1c). In concurrence with the printed pattern diameter, the transmitted intensity remains nearly the same for higher irradiation time scales (>400 s). Herein, the printing of plasmonic nanoparticles occurs due to the resonance plasmonic absorption of the optical radiation from the projector lamp. The absorption of optical radiation by the plasmonic nanoparticles creates a temperature gradient along the propagation direction due to the photothermal conversion of the absorbed light. The temperature gradient generates a thermally induced convective flow and drags the particles toward the irradiation zone along the fluid flow, wherein they assemble and anchor to the substrate *via* van der Waal's force. Herein, the diameter of the printed zone is determined by the strength of thermally induced convective flow to bring the nanoparticles towards the irradiation zone, and it explains the plateau region in Fig. 1b. At lower irradiation time scales, more and more plasmonic nanoparticles are dragged toward the irradiation zone, reducing the transmitted intensity. However, at larger timescales, the force from the thermal convective flow is insufficient for more particles laterally and along the *z*-direction, so the transmitted intensity remains nearly the same.

The potential of the optically printed plasmonic pattern for optothermally trapping the yeast cells from a colloidal droplet solution is explored, and the results are shown in Fig. 2a(i–iii) and Video S1. Herein, the optothermal trapping zone is printed using a 100× objective by exposing the Ag colloidal solution for 30 seconds with light from the projector lamp (12 µW power). The printed region has a dimension of ~5 µm that matches the particle dimension (~4 µm), so that upon trapping, the illumination region can be masked by the trapped objects to ensure the trapping. Herein, following the optical printing of the plasmonic particles, the printed region is cleaned by washing and ultrasonication before putting the yeast cell solution. The printed zone is then illuminated with optical radiation from the projector lamp, and the photothermal conversion of light into heat results in the thermal convection of fluid around the heating zone, and drags the yeast cells towards the irradiation zone. The trapped cells are found to remain in the optothermal trap even after exposure for 10 minutes (Video S1), and upon switching off the illumination, the yeast cells re-disperse into the solution (Fig. 2a(iv–v)). The velocity profile of the trapped cells is estimated from the video images using the ImageJ software, and the obtained velocity profile is shown in Fig. S1. In concurrence with the earlier studies, the velocity of the cells increases as they come closer to the irradiation zone. The long-range thermophoretic dragging capability of the printed patterns (12 µW excitation power for a 30 second duration) of dimension 5 µm can be used to move the objects across the surface by printing patterns of the desired shape. Herein, we created a 3 × 3 array of printed patterns of dimensions 30 µm × 30 µm that are separated by a centre-to-centre distance of 12 µm. Initially, a yeast trapped to spot 1 and then moved in the pattern of letters N (Fig. 2bi–iv) and Z (Fig. 2bv–viii) by alternately exposing the printed spots of interest. The measured velocity of the object is found to be ~0.9 µm s^{-1} between two adjacent patterns and it is ~0.77 µm s^{-1} while moving diagonally. This clearly illustrates the potential of sequential excitation of the printed zones not only to trap the objects but also to manipulate across the desired shapes, and this tweezing potential of the
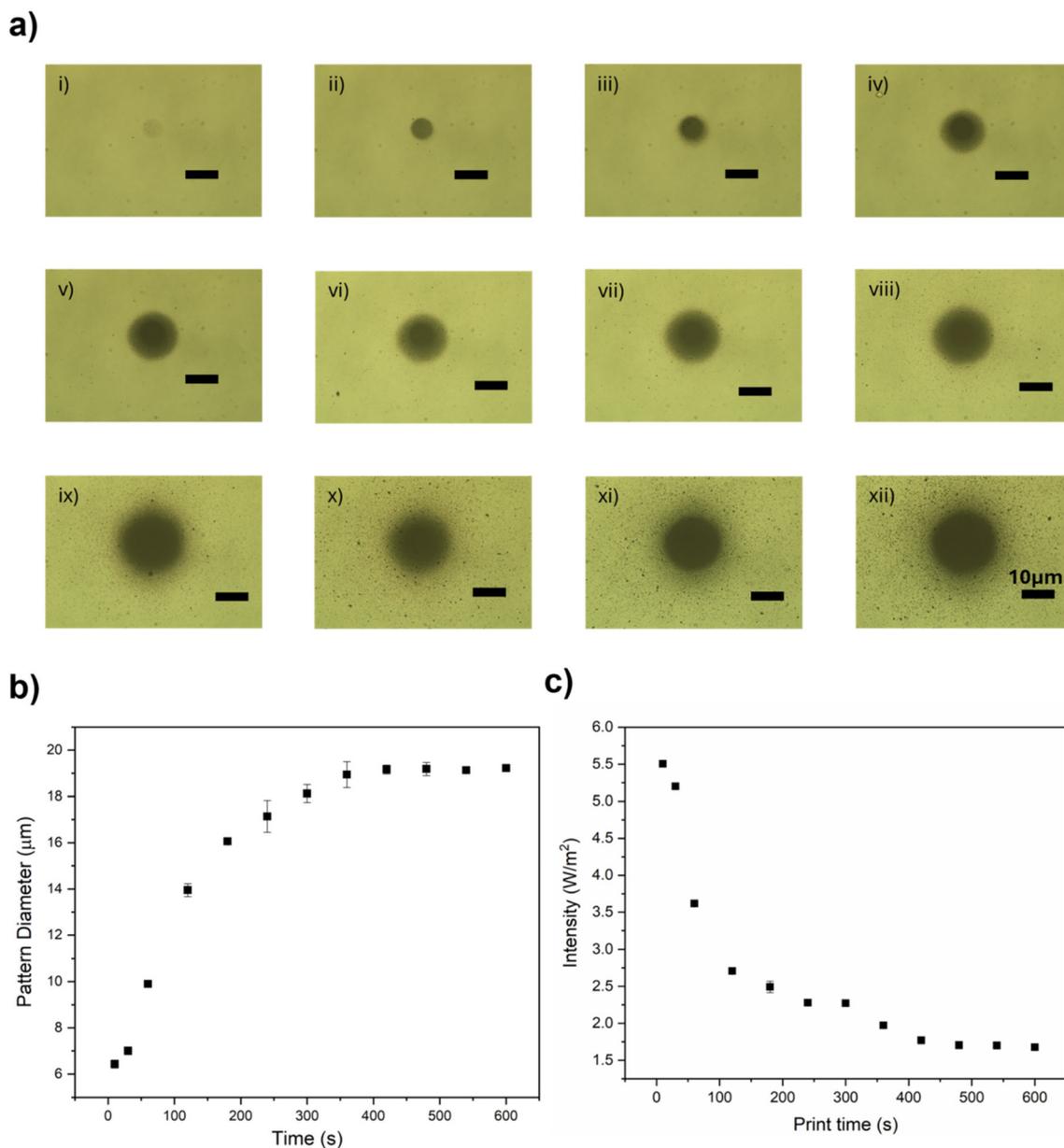
Fig. 1 (a) Temporal evolution of printed silver patterns for the print times (i) 10 s, (ii) 30 s, (iii) 60 s, (iv) 120 s, (v) 180 s, (vi) 240 s, (vii) 300 s, (viii) 360 s, (ix) 420 s, (x) 480 s, (xi) 540 s, and (xii) 600 s (scale: 10 μm). (b) Temporal variation of the print size of silver nanoparticles. (c) Variation of transmission p to the print time of the printed nanoparticle.

optothermal trap *via* selectively optically exciting the printed pattern is not much explored so far.

Contrary to the laser-assisted optothermal localized heating and trapping of the object, the white light illumination allows the excitation of multiple printed patterns at desired locations and parallel trapping of multiple objects at this location, as shown in Fig. 3. Herein, among the three printed zones, the 1st and 3rd are irradiated with optical radiation, and the optothermal trapping of a silica particle and a yeast cell onto these zones is observed while there is no movement of particles towards the 2nd patterned region. Similarly, by irradiating the

2nd pattern, the trapping of multiple particles, the yeast cell and the silica particle, onto the same trap is also observed. This could be useful in studying particle–particle or biological cell–biological cell interactions.

In this study, the maximum trapping velocity of yeast cells was found to be ~2.7 μm s^{-1}. An increase in the projector illumination power is expected to further enhance this velocity. Table 1 provides a summary of non-laser-based trapping approaches on plasmonic substrates, with the first entry demonstrating manipulation without the use of a laser. Given the limited reports on non-laser-based manipulation with plas-
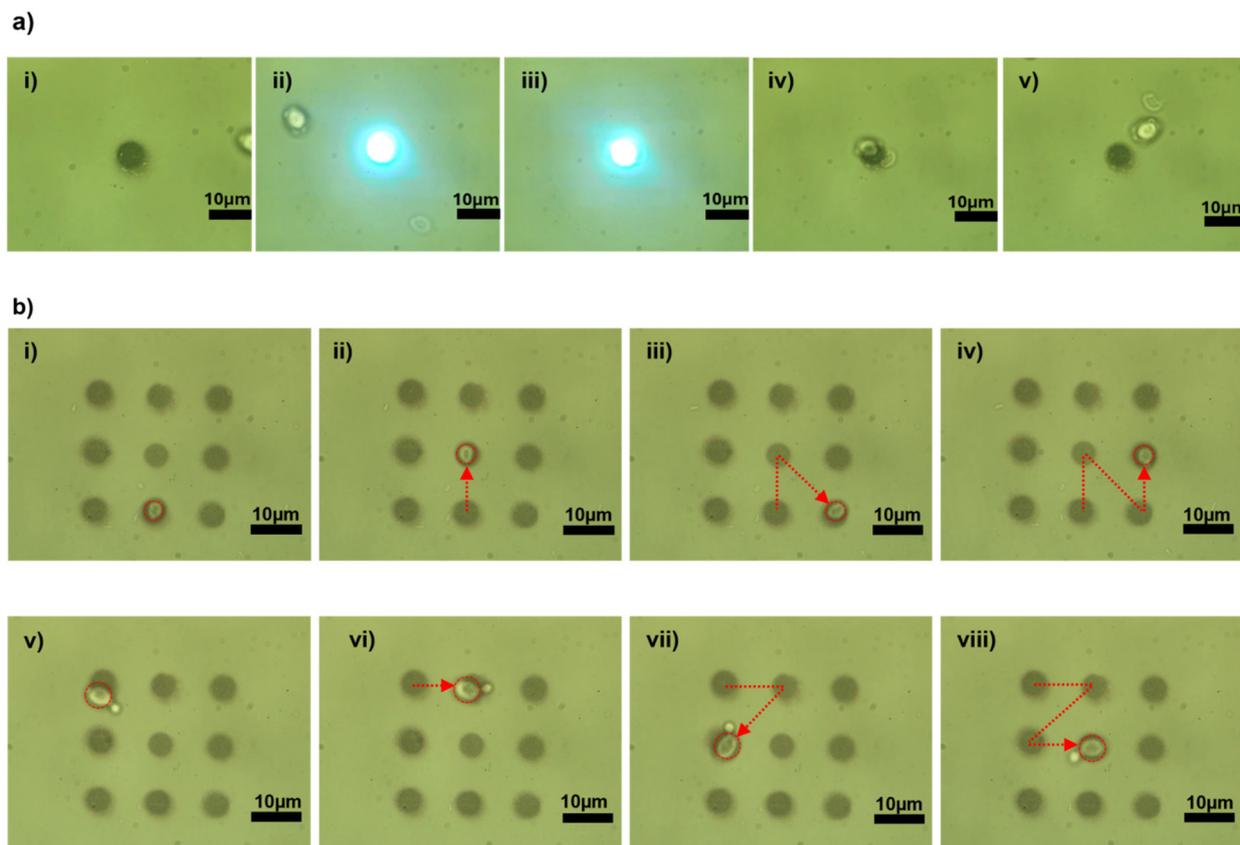
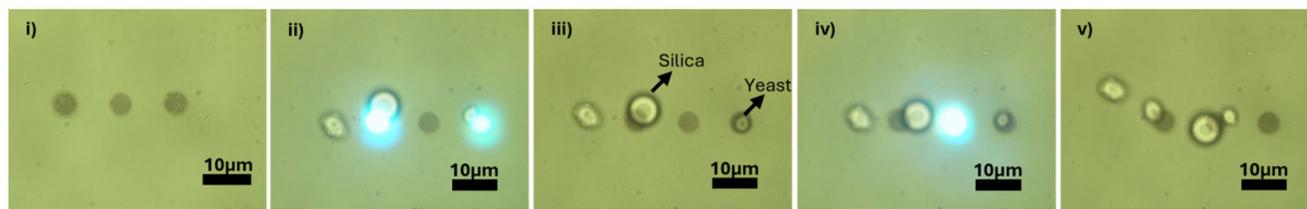**Fig. 2** (a) Optothermal trapping of yeast cells and (b) optothermal lateral manipulation of a yeast cell.

Fig. 3 Optothermal parallel trapping of silica particles and yeast cells.

Table 1 Microparticle velocity profiles under various manipulation techniques on a plasmonic substrate

Technique	Particle type & size	Manipulation speed
Electrothermoplasmonic steering[37]	PS microspheres (1 μm)	2.2 μm s^{-1}
SPP-based plasmonic transport[38]	PS microspheres (≈5–10 μm)	1.94–4.56 μm s^{-1}
Photophoretic movement[39]	Gold micro-plate	~30 μm s^{-1}
Current study	Yeast (~5 μm)	~2.7 μm s^{-1}

monic substrates, a few laser-assisted methods utilizing alternative trapping mechanisms are also included for comparison.

Finally, the surface enhancement Raman scattering capability of the printed plasmonic region is evaluated by printing a rectangle of dimensions 2 mm × 1 mm using a 4× microscope objective. Herein, the plasmonic regions are printed for different time scales, ranging from 11 to 15 minutes in steps of 1-minute increments. A 10 μl droplet of 10 μM crystal violet is dispensed onto the substrate. Owing to the high hydrophilicity of the printed region and the glass substrate, the crystal violet droplet spreads to the surface (Fig. S2) and forms a coffee ring effect upon evaporation. Using a micro-Raman setup, the Raman signal of crystal violet is measured across the coffee ring for the substrates printed at different time scales. The average Raman spectra of ten measurements of crystal violet on these substrates using the micro-Raman setup are recorded and shown in Fig. 4a. The assignment done for
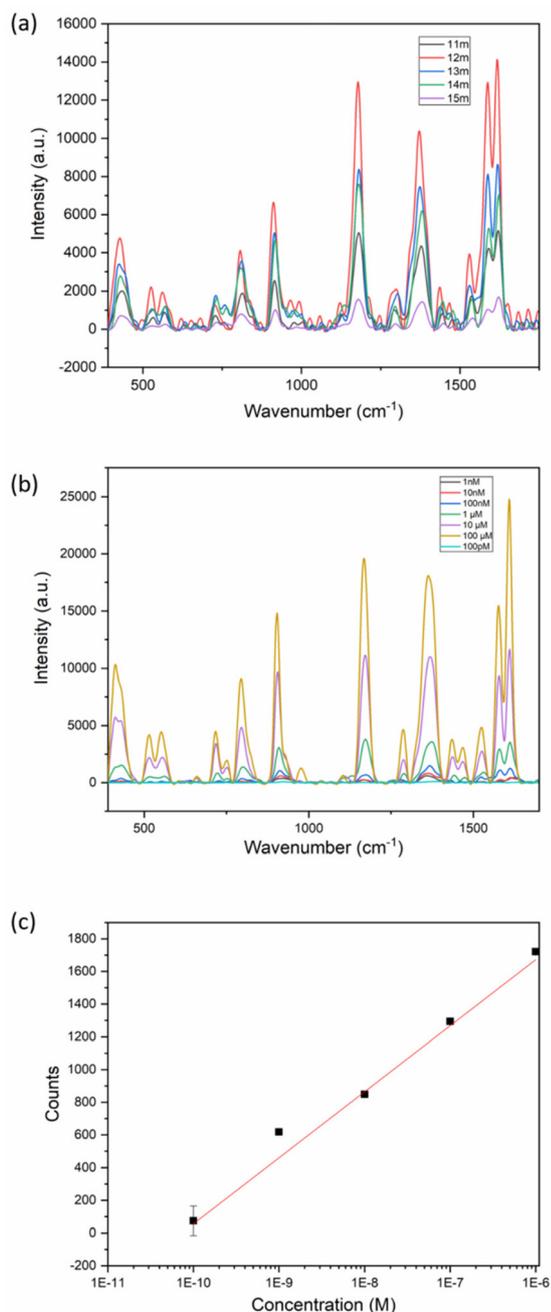
Fig. 4 (a) Surface-enhanced Raman spectra of crystal violet on various time printed silver patterns, (b) surface-enhanced Raman spectra of CV of various concentrations on 12-minute printed silver, and (c) concentration *vs.* counts plot for the peak 1360 cm^{-1} of CV.

Table 2 SERS detection limits for different non-laser plasmonic printing methods

Substrate method	Probe molecule	Limit of detection
Inkjet (Ag NP on paper)[43]	R6G	~10 fM
Inkjet (Ag on chitosan-paper)[44]	R6G	10.7 pM
Screen printing (Ag NP arrays)[45]	R6G	100 nM
Microcontact-printing (Au NP)[46]	miRNA-21	11.96 fM
Current study	Crystal violet	62 pM

enhancement. Furthermore, an increase in the printed region resulted in a much closer printing of the plasmonic nanoparticles that could lead to the quenching of the Raman signal rather than enhancement. Furthermore, the Raman signal of the various concentrations of the crystal violet was measured on the plasmonic substrate printed for 12 minutes, and the results obtained are shown in Fig. 4b. It is observed that the printed substrate exhibits well-defined Raman peaks for concentrations as low as 100 pM. The limit of detection of the present approach was estimated using the 1360 cm^{-1} peak of the crystal violet by using the equation $y = Y_B + 3S_B$,[42] where the R-squared value is 0.9887, is found to be 62 pM.

Table 2 summarizes selected studies on non-laser-based plasmonic nanoparticle printing methods and their corresponding SERS yields, benchmarked against the results of the present work.

Experimental observations confirm the reproducibility of the printed patterns. As shown in Fig. S4, ten consecutive trials with identical printing conditions consistently produced a pattern diameter of ~11 μm. Furthermore, at a Raman shift of 805 cm^{-1} for crystal violet dye, the mean Raman intensity was measured as 543 ± 22 counts.

Conclusions

In summary, we have demonstrated a white-light-assisted approach for the optical printing of plasmonic nanoparticles and their utilization for optothermal trapping and manipulation of microscopic objects such as yeast cells and silica particles. A study on the temporal evolution of the printed plasmonic regions revealed that the printed spot diameter reached a plateau region beyond a certain optical radiation exposure duration and the transmittance study concurs with the results and confirms that the printing happens more in a 2D fashion. The utility of the printed plasmonic pattern was demonstrated by optothermal trapping of the yeast cell under white light illumination. Moreover, we illustrated optothermal trapping of multiple objects at various locations onto the same substrate for the first time by selectively exposing the printed plasmonic pattern. Furthermore, by selectively exciting multiple printed zones, we achieved parallel trapping and dynamic tweezing, enabling controlled motion of trapped objects along predefined paths. Additionally, we explored the surface-enhanced Raman spectroscopic (SERS) capabilities of the printed plas-

the Raman peaks is depicted in Table S1.[40,41] From Fig. 4a, it is observed that the substrate printed for 12 minutes exhibited maximum signal enhancement. The results obtained are further corroborated by FESEM studies (Fig. S3). The FESEM studies elucidated that there is a gap between the printed particles for 12 minutes, whereas the printed particles are so close to each other for printed plasmonic regions that the probe molecule resided on the hotspots to provide maximum signal

monic regions, and it was found that maximum Raman signal enhancement occurred for the substrate printed for 12 minutes. The optimized substrate exhibited the highest enhancement, achieving a detection limit as low as 62 pM for crystal violet, highlighting the potential of this method for ultrasensitive molecular detection. The ability to dynamically control and manipulate objects using selectively excited printed plasmonic patterns presents exciting prospects for lab-on-a-chip technologies, biophotonics, and advanced optical tweezing applications.

Materials and methods

Materials

$AgNO_3$ (99.0%, Loba Chemie Private Limited, India), tri-sodium citrate dihydrate (98%, Loba Chemie Private Limited, India), crystal violet (88%, Loba Chemie Private Limited, India), yeast (Grain 'N' Grace Food Ingredients Manufacturing Private limited, India), and silica (5% w/v, Spherotech, USA) were used.

Synthesis of Ag nanoparticle solution

The Ag nanoparticle colloidal solution was prepared *via* the Lee and Meisel method.[47] Briefly, 17 mg of $AgNO_3$ was dissolved in 50 ml of deionized water and placed on a hotplate maintained at 100 °C. Then, a 40 mM solution of trisodium citrate was added dropwise to the solution and stirred magnetically until the color changed to golden yellow. The absorption spectra of the synthesized Ag nanoparticles were recorded using a UV/Visible spectrophotometer (JASCO V650), exhibiting a peak centred at 430 nm, as shown in Fig. S5. The zeta potential of the prepared particle is measured using a Horiba particle size analyser and was determined to be −12.1 mV with the particle size of 44 nm, as shown in Fig. S6.

Preparation of yeast cell solution

A yeast cell solution with a concentration of 0.1 mg ml^{-1} was prepared by dissolving dried yeast in water at room temperature.

Experimental setup

A commercial LCD projector (BenQ MX560 XGA) with a maximum brightness of 4000 lumens was used for the printing setup (Fig. S7). The projector was employed as the illumination source owing to its broad spectral emission profile (Fig. S8), which exhibits strong overlap with the wide absorption band of the nanosilver colloid solution. The diverging light beam from the projector was collimated using the microscope eyepiece and then passed through a simple Galilean lens arrangement consisting of a plano concave lens and a biconvex lens of focal lengths of −150 mm and 300 mm, respectively, to tune the image magnification. The light was then coupled to an inverted microscope configured with a beam splitter and a microscope objective (100× oil immersion

objective (NA = 1.45)). A 4× objective (NA = 0.10) is used instead of a 100× objective for spectroscopic study. Printing was performed on a glass coverslip placed on the sample stage. The Nikon Eclipse Ti2 inverted microscope was used for coupling the optical radiation for the printing and imaging of the pattern. The field-enhanced scanning electron microscopy images of the printed patterns were recorded using Nova NanoSEM. To record the Raman spectrum, a 532 nm laser was coupled through the microscope and the Raman signals from the sample were captured using a Horiba Scientific iHR-320 spectrometer.

Author contributions

The manuscript was written through contributions of all authors. All authors have given approval to the final version of the manuscript.

Conflicts of interest

There are no conflicts to declare.

Data availability

Data will be available from the corresponding author upon request.

Supplementary information is available. Contents: Fig. S1: velocity of yeast cells as a function of radial distance from the printed plasmonic pattern. Fig. S2: CV dried on 4× objective assisted printed silver patterns for the print time, (a) 11 min, (b) 12 min, (c) 13 min, (d) 14 min, (e) 15 min (scale bar: 100 μm). Fig. S3: FESEM images of the silver nanoparticles for the print time, (a) 11 min, (b) 12 min, (c) 13 min, (d) 14 min, (e) 15 min (inset: magnified images of the patterns). Fig. S4: (a) Projector assisted printed silver patterns (scale bar: 10 μm), (b) Trial *vs.* Diameter plot of the printed patterns, (c) Trial *vs.* Intensity counts for the Raman shift of 805 cm^{-1} for crystal violet. Fig. S5: UV–Vis absorption spectrum of prepared Ag colloidal solution. Fig. S6: (a) particle size distribution showing an average particle size of ~44 nm. (b) Zeta potential measurement suggests a net negative surface charge on the particles. Fig. S7: schematic of the projection printing setup. See DOI: **https://doi.org/10.1039/d5nr01955a**.

References

1 A. S. Urban, A. A. Lutich, F. D. Stefani and J. Feldmann, *Nano Lett.*, 2010, **10**, 4794–4798.

2 J. Li, E. H. Hill, L. Lin and Y. Zheng, *ACS Nano*, 2019, **13**, 3783–3795.

3 R. J. Barsotti, M. D. Vahey, R. Wartena, Y. M. Chiang, J. Voldman and F. Stellacci, *Small*, 2007, **3**, 488–499.

4 M. Janjua, S. Nudurupati, P. Singh and N. Aubry, *Electrophoresis*, 2011, **32**, 518–526.

5 B. B. Yellen, O. Hovorka and G. Friedman, *Proc. Natl. Acad. Sci. U. S. A.*, 2005, **102**, 8860–8864.

6 Y. Sahoo, M. Cheon, S. Wang, H. Luo, E. P. Furlani and P. N. Prasad, *J. Phys. Chem. B*, 2004, **108**, 3380–3383.

7 H. Sazan, S. Piperno, M. Layani, S. Magdassi and H. Shpaisman, *J. Colloid Interface Sci.*, 2019, **536**, 701–709.

8 W. Liu, H. Gao, K. Liu, D. Lei, K. Pei and G. Hu, *J. Nanopart. Res.*, 2022, **24**, 81.

9 J. Do, K. N. Sediq, K. Deasy, D. M. Coles, J. Rodríguez-Fernández, J. Feldmann and D. G. Lidzey, *Adv. Opt. Mater.*, 2013, **1**, 946–951.

10 L. P. Martinez, S. Poklepovich-Caride, J. Gargiulo, E. D. Martínez, F. D. Stefani, P. C. Angelomé and I. L. Violi, *Nano Lett.*, 2023, **23**, 2703–2709.

11 E. H. Hill, C. Goldmann, C. Hamon and M. Herber, *J. Phys. Chem. C*, 2022, **126**, 7622–7629.

12 F. Zacharatos, M. Duderstadt, E. Almpanis, L. Patsiouras, K. Kurselis, D. Tsoukalas, C. Reinhardt, N. Papanikolaou, B. N. Chichkov and I. Zergioti, *Opt. Laser Technol.*, 2021, **135**, 106660.

13 Y. Zhang, Z. Liang, A. P. Zhang and H. Y. Tam, *Adv. Opt. Mater.*, 2021, **9**, 2001368.

14 T. Xu, Y. Qi, X. Zhao and Q. Zhang, *Colloids Surf., A*, 2016, **498**, 139–145.

15 F. Schuknecht, C. M. Maier, P. Vosshage, V. A. Hintermayr, M. Döblinger and T. Lohmüller, *Nano Lett.*, 2023, **23**, 4762–4769.

16 J. Zheng, X. Cheng, H. Zhang, X. Bai, R. Ai, L. Shao and J. Wang, *Chem. Rev.*, 2021, **121**, 13342–13453.

17 Y. Liu, M. Kim, S. H. Cho and Y. S. Jung, *Nano Today*, 2021, **37**, 101063.

18 B. Zhang, X. Zhang, J. Luo, S. Liu and Y. Tian, *Opt. Mater.*, 2023, **143**, 114233.

19 G. Wu, J. Zhu, G. Weng, J. Li and J. Zhao, *Microchim. Acta*, 2021, **188**, 345.

20 G. Zheng, S. Mourdikoudis and Z. Zhang, *Small*, 2020, **16**, 2002588.

21 M. J. Guffey and N. F. Scherer, *Optical Trapping and Optical Micromanipulation VII*, 2010, vol. 7762, p. 77623H.

22 M. J. Guffey, R. L. Miller, S. K. Gray and N. F. Scherer, *Nano Lett.*, 2011, **11**, 4058–4066.

23 S. Nedev, A. S. Urban, A. A. Lutich and J. Feldmann, *Nano Lett.*, 2011, **11**, 5066–5070.

24 K. Monisha, K. Suresh, A. Bankapur and S. D. George, *Sens. Actuators., B*, 2023, **377**, 133047.

25 K. Monisha, K. Suresh, A. Bankapur and S. D. George, *Anal. Chim. Acta*, 2024, **1317**, 342903.

26 C. M. Jin, W. Lee, D. Kim, T. Kang and I. Choi, *Small*, 2018, **14**, 1803055.

27 M. C. Wu, *Nat. Photonics*, 2011, **5**, 322–324.

28 J. Li and Y. Zheng, *Acc. Mater. Res.*, 2021, **2**, 352–363.

29 P. S. Kollipara, Z. Chen and Y. Zheng, *ACS Nano*, 2023, **17**, 7051–7063.

30 X. Zeng, Y. Nyquist, Q. Zhang, H. J. Butt and S. Wu, *Supramol. Mater.*, 2022, **1**, 100004.

31 A. Swain, P. S. Kollipara and Y. Zheng, *J. Phys. Chem. C*, 2024, **128**, 7316–7322.

32 M. Herber, D. Lengle, S. R. Valandro, M. Wehrmeister and E. H. Hill, *Nano Lett.*, 2023, **23**, 6308–6314.

33 Y. Xie, S. Yang, Z. Mao, P. Li, C. Zhao, Z. Cohick, P. H. Huang and T. J. Huang, *ACS Nano*, 2014, **8**, 12175–12184.

34 J. E. George, V. K. Unnikrishnan, D. Mathur, S. Chidangil and S. D. George, *Sens. Actuators, B*, 2018, **272**, 485–493.

35 A. Peethan, M. Aravind, V. K. Unnikrishnan, S. Chidangil and S. D. George, *Appl. Surf. Sci.*, 2022, **571**, 151188.

36 B. Bannur, K. Monisha, S. M. Shivalingegowda and S. D. George, *Mater. Horiz.*, 2025, **12**, 4875–4883.

37 H. Cong, J. Chen and H. P. Ho, *Sens. Actuators, B*, 2018, **264**, 224–233.

38 X. Peng, A. Kotnala, B. B. Rajeeva, M. Wang, K. Yao, N. Bhatt, D. Penley and Y. Zheng, *Adv. Opt. Mater.*, 2021, **9**, 2100050.

39 J. Li, A. Alfares and Y. Zheng, *iScience*, 2022, **25**, 104035.

40 A. Cesaratto, J. R. Lombardi and M. Leona, *J. Raman Spectrosc.*, 2017, **48**, 418–424.

41 J. Wu, J. Fang, M. Cheng and X. Gong, *Appl. Phys. A*, 2016, **122**, 844.

42 V. Puravankara, A. Manjeri, M. M. Kulkarni, Y. Kitahama, K. Goda, P. K. Dwivedi and S. D. George, *Anal. Chem.*, 2024, **96**, 9141–9150.

43 W. W. Yu and I. M. White, *Anal. Chem.*, 2010, **82**, 9626–9630.

44 T. T. Thuy, M. Sharipov, Y. Lee, B. T. Huy and Y. Lee, *Nano Select*, 2020, **1**, 499–509.

45 C. McDonnell, F. M. Albarghouthi, R. Selhorst, N. Kelley-Loughnane, A. D. Franklin and R. Rao, *ACS Omega*, 2023, **8**, 1597–1605.

46 H. Li, H. Zhang, W. Luo, R. Yuan, Y. Zhao, J.-A. Huang and X. Yang, *Anal. Chim. Acta*, 2022, **1229**, 340380.

47 P. C. Lee and D. Meisel, *J. Phys. Chem.*, 1982, **86**, 3391–3395.